Few-Reference Image Quality Assessment with Multiple Information Measurement Fusion

Shuang Shi[1,2,3,4,5], Simeng Wang[1,2,3,4,5], Yuchen Liu[1], Chengxu Zhou[1,2,3,4,5,6,7(✉)], and Ke Gu[1,2,3,4,5]

[1] Faculty of Information Technology, Beijing University of Technology, Beijing, China
zhouchengxu@lnut.edu.cn
[2] Engineering Research Center of Intelligent Perception and Autonomous Control, Ministry of Education, Beijing, China
[3] Beijing Laboratory of Smart Environmental Protection, Beijing, China
[4] Beijing Key Laboratory of Computational Intelligence and Intelligent System, Beijing, China
[5] Beijing Artificial Intelligence Institute, Beijing, China
[6] School of Electronic and Information Engineering, Liaoning University of Technology, Jinzhou, Liaoning, China
[7] Key Laboratory of Intelligent Control and Optimization for Industrial Equipment of Ministry of Education, Dalian University of Technology, Dalian, China

Abstract. In the era of media information explosion, there is an urgent need for a fast and reliable image quality assessment (IQA) model to improve the actual application effect of images. To this end, we propose the multiple information measurement fusion metric (MMFM), which innovatively combines two types of information measures (IMs), i.e., local IM and global IM, using only a small number of references for IQA. First, inspired by the free energy theory, we combine 2-dimensional autoregressive model with sparse random sampling method as an inference engine on an input image to generate its associated predicted image. Second, by the inspiration of pixel-wise measurement, we obtain the local IM by calculating the information entropy of the residual error between the input image and its corresponding predicted one. Third, motivated by the histogram-based measurement, we acquire the global IM by computing the two kinds of divergences between the input image and its predicted one. Fourth, we systematically fuse three components, independently including one distance of local IM between the reference and corrupted images and two distances of global IMs between the reference

This work was supported in part by the Beijing Natural Science Foundation under Grant JQ21014; in part by the National Science Foundation of China under Grant 62273011 and Grant 62076013; in part by the Industry-University-Research Innovation Fund for Chinese University - Blue Point Distributed Intelligent Computing Project under 2021LDA03003; in part by the Ministry of Education of China under Grant 202102535002, Grant 202102535012; in part by the Key Laboratory of Intelligent Control and Optimization for Industrial Equipment of Ministry of Education, Dalian University of Technology under Grant LICO2022TB03.

G. Zhai et al. (Eds.): IFTC 2022, CCIS 1766, pp. 258–269, 2023.
https://doi.org/10.1007/978-981-99-0856-1_19

and corrupted images, based on a linear function to derive the final IQA result. The results of experiment on the most popular LIVE database show that our designed algorithm with only one number used as few reference has achieved well performance as compared with several mainstream IQA models.

Keywords: Free energy theory · Image quality assessment · Few reference · Information measurement fusion

1 Introduction

Currently, the speed of information dissemination is extremely fast by various media, enabling everyone to obtain a huge number of images or video frames every minute. A vast quantity of visual data is easily corrupted by aliasing, blurring, noise, etc., in the process of generation, storage, transmission and consumption. In this case, it is too costly and inefficient to rely on a large amount of human labor for monitoring and controlling the quality of an image or a video frame. Therefore, an automatic system that can quickly and accurately evaluate visual data is urgently needed [1]. The image quality assessment (IQA) approach is considered as the best solution confronting this situation, which adopts computer techniques has excellent perception ability to obtain visual quality.

Generally, the IQA methods are divided into objective and subjective assessment methods [2–5]. The subjective IQA method is an accurate evaluation method that plays an important role, since it can provide the testing data and its truth quality scores (such as LIVE [6]) for corroborating the precision of objective IQA methods. However, subjective IQA method highly relies on human observers, and thus is laborious, time-wasting, high-costing and cannot be used in real-time applications. So, there is a growing promotion of the objective IQA methods to speed up and precisely evaluate the image quality by adopting multifarious mathematical models. Based on the utilization of the original image information, the objective IQA methods are further divided into three classes, that is full-reference (FR), reduced-reference (RR) and no-reference (NR). The FR IQA method is supposed to utilize complete original image information, like famous mean squared error (MSE), structural similarity index (SSIM) [7], feature similarity (FSIM) [8], etc. In the existing researches [9–20], the primary designing principle of the most FR IQA methods is based on extreme sensitivity of the human visual system (HVS) to the degradation of image structure. Nevertheless, we cannot guarantee that the entire original image information is always available, which makes the application scopes of FR methods greatly narrow. The RR IQA methods [21–26] use a portion of the referenced image information and the NR methods [15,27–38] rely on statistical rules without using any original information, attracting more and more attention. It is worth noting that the free energy-based IQA algorithm can highly simulate the process of human visual perception, so it has been widely studied by peers. For instance, the free energy based distortion metric (FEDM) gets inspirations from the free energy theory to estimate the human internal generative (IG) model [39,40].

Although a great quantity of IQA algorithms were proposed, only a minority of algorithms (such as MSE and SSIM) can be commendably embedded into pre-existing image/video image processing systems due to the restriction of computational complexity, portability and the demand of the whole referenced image [41]. Aiming at these limitations, we designed a valid IQA method, named multiple information measurement fusion metric (MMFM), considering both local and global information metrics (IMs). The designed MMFM has the characteristics of stronger portability and less computation, deserving great potential of development and wide application prospects. It is worth emphasizing that MMFM can be considered as a reference-free IQA model, since it just requires one number as an RR IQA feature and this number can be precisely encoded in a header file with relatively minor bits.

The remainder of this paper is arranged as follows. In Sect. 2, we present five specific steps of the MMFM model in detail. In Sect. 3, we conduct comparative experiments with typical FR and RR algorithms on the famous LIVE database. The results show that the proposed algorithm has comparable performance with some mainstream FR and RR algorithms. In Sect. 4, we introduce the areas where the model can be applied. In Sect. 5, we finally summarize all the work.

2 Methodology

In most cases, humans can perceive visual signals through specific mechanisms, which have been shown to be strongly associated with neural circuits in the primate visual cortex. This paper fuses a local IM and two global IMs to obtain MMFM. Its framework is shown in Fig. 1. The main rationale behind the proposed MMFM is that the image with more valuable information can help for evaluating image quality.

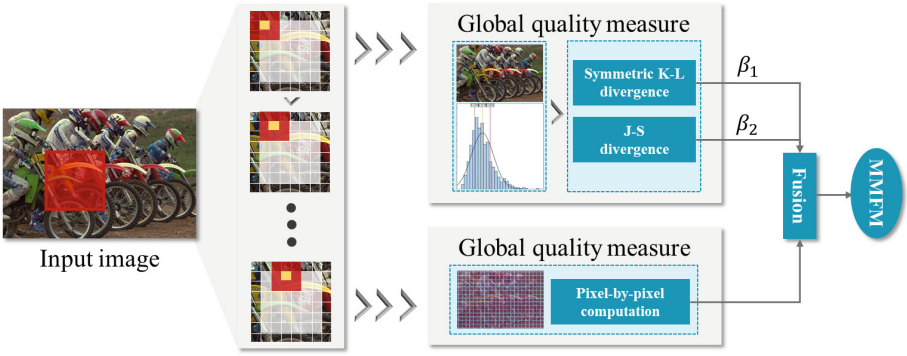

Fig. 1. Basic framework of our designed MMFM model.

2.1 Free Energy Measurement

The most mainstream IQA models focus on extracting low-level features, including structural information, image gradient, and phase congruency. We have faith

that the image quality is highly related with the human brain's perception mechanisms on the psychological and physiological. During the past few years, Friston came up with a landmark theory called the free energy theory based on human perception, demonstrating multiple brain principles including human perception, thinking, behavior and learning from biological and physical scientific perspectives. The free energy theory depends on the IG model control to achieve accurate cognition, which is very like the Bayesian brain hypothesis extensively used in ensemble learning [42]. Specifically, the IG model indicates that the human brain can understand, interpret and forecast those external visual scenes in a constructive way. In effect, the IG model is a probabilistic model containing a likelihood term and a prior term, which can be utilized to categorize the input images into ordered part and unordered part. For the follow-up work, the two parts can be well embedded into the process of analysis, detection, and identification, etc.

First, we consider the internal generative model G as a parameterized model of visual perception. The IG model can explain the perceptual scenes by changing the vector $\mathbf{m}$ of parameters. The "surprise" of an input image I is assessed by joint distribution $J(I, \mathbf{m}|G)$ integral on the model parameters $\mathbf{m}$:

$$-\log J(I|G) = -\log \int J(I, \mathbf{m}|G) d\mathbf{m}. \tag{1}$$

Then, we add an auxiliary term $A(\mathbf{m}|I)$ into Eq. (1) to obtain:

$$-\log J(I|G) = -\log \int A(\mathbf{m}|I) \frac{J(I, \mathbf{m}|G)}{A(\mathbf{m}|I)} d\mathbf{m}. \tag{2}$$

By utilizing Jensen's inequality, Eq. (2) can be rewritten as

$$-\log J(I) \leq -\int A(\mathbf{m}|I) \log \frac{J(I, \mathbf{m})}{A(\mathbf{m}|I)} d\mathbf{m}. \tag{3}$$

So, the right-hand side of Eq. (3) is a maximum term called "free energy", which is defined as

$$F(\mathbf{m}) = -\int A(\mathbf{m}|I) \log \frac{J(I, \mathbf{m})}{A(\mathbf{m}|I)} d\mathbf{m}. \tag{4}$$

2.2 Sparse Random Sampling

Based on Attias research, the famous linear autoregressive (AR) model can minimize free energy, which is resemblance to the predictive coding [43]. The AR model can approximate a wide range of natural scenes by changing the parameters. Thus, we utilize the AR model to simply represent the IG model of the free energy theory for making analysis of the input image I. The location and value of pixel are defined as a and p_a. The relationship between this pixel information and its surrounding information can be expressed as

$$p_a = \Gamma_\theta(p_a)\mathbf{n} + \sigma_a \tag{5}$$

where $\Gamma_\theta(p_a)$ is an adjacent vector covering its neighborhoods θ pixels in the local $(\theta+1)^{\frac{1}{2}} \times (\theta+1)^{\frac{1}{2}}$ block, $\mathbf{n} = (\mathbf{n}_1, \mathbf{n}_2, ..., \mathbf{n}_\theta)^T$ is a vector of AR coefficients, and σ_a is the white noise with a mean of zero:

$$q_a = \mathbf{n_{est}} \Gamma_\theta(p_a) \tag{6}$$

where q_a is the predicted pixel value corresponded to p_a, and the $\mathbf{n_{est}}$ is the optimal predictive value of AR coefficient for p_a.

To obtain the optimal vector of AR coefficient, we consider the linear system as a matrix way:

$$\mathbf{n_{est}} = \arg\min_{\mathbf{n}} ||\mathbf{y} - \mathbf{Y}\mathbf{n}||_2 \tag{7}$$

where $\mathbf{y}$ on behalf of the transpose vector of $(p_a^1, p_a^2, ..., p_a^\gamma)$, and $\mathbf{Y}(l,:) = \Gamma_\theta(p_a, l)$, among which $l > 1$, $l \in [1,l]$ is spaced by one.

Then the least square approach is embedded into Eq. (7), and we finally obtain the best AR coefficient as follows:

$$\mathbf{n_{est}} = (\mathbf{Y}^T\mathbf{Y})^{-1}\mathbf{Y}^T\mathbf{y}. \tag{8}$$

The current proposed IQA model on the basis of free energy theory can obtain great performance, but requires a lot of CPU running time. To promote efficiency of implementation, we design a low time-consuming and high performance method by introducing the sparse random sampling method. In this work, the method of sparse random sampling is used to conduct 28 samplings from 1/1,000 pixels to an entire input image. It is particularly worthy to mention that the method of extremely sparse random sampling implements pretty quickly and is able to extensively inserted into the most image processing systems. The preponderance of the method of sparse random sampling makes the proposed IQA model more flexible and practical.

2.3 Local Information Measurement

Motivated by the pixel-wise measurement, we calculate the information entropy of the residual error between the input image and the predicted one. The r_a in the residual map r is related to p_a, which can be obtained by canceling the predicted pixel:

$$r_a = p_a - q_a. \tag{9}$$

To sum up, by calculating the entropy of the residual map, the free energy value F of the input image can be rewritten as

$$F = -\int_b r(b)\log r(b)db \tag{10}$$

where *r(b)* indicates the probability density of grayscale *b*. Accordingly, we define the perceptual distance D between the reference image I_R and the corresponding corrupted image I_C. By using Eq. (10), we can obtain:

$$D = |F_R - F_C| \tag{11}$$

where F_R and F_C correspond to the free energy values of I_R and I_C, respectively.

2.4 Global Information Measurement

The entropy of image ignores the influence of pixel position and only considers the distribution of pixel values. The uniform degree of image's histogram distribution reflects the amount of information contained in the image. The image N' with completely uniform histogram distribution contains the most information. As the gap between the histogram of the input image N_I and that of the image N' decreases, the global information of N_I increases.

The difference of histogram information between N_I and N' is computed by

$$\Delta F = F(N_I) - F(N') = \sum N_I(b) \log N_I(b) - \sum N'(b) \log N'(b). \tag{12}$$

Since it cannot explain the interrelation between two images, we select a commonly used distance measure method named the Kullback-Leibler (K-L) divergence. N_O is the histogram of predicted image. The K-L divergence between the given two probability N_I and N_O can be calculated:

$$D_{KL}(N_I, N_O) = -\sum N_O(b) \log N_I(b) + \sum N_I(b) \log N_O(b). \tag{13}$$

By using K-L divergence, the interaction between N_I and N_O is also commendably considered. However, in practical applications, the order of K-L divergence's arguments may cause the results to change substantially [44]. Therefore, we introduce a symmetric variant of asymmetric K-L divergence to measure distance, which can be obtained by:

$$D'_{KL}(N_I, N_O) = \frac{D_{KL}(N_I, N_O) + D_{KL}(N_O, N_I)}{2}. \tag{14}$$

In addition to the symmetric variant of the K-L divergence, many symmetric forms have been proposed, such as Jensen-Shannon (J-S) divergence, arithmetic mean, geometric mean, harmonic mean and so on [40]. In our work, we select the typical J-S divergence because of its symmetric and smooth format:

$$D_{JS}(N_I, N_O) = \frac{D_{KL}(N_I, N) + D_{KL}(N_O, N)}{2} \tag{15}$$

where $N = (N_I + N_O)/2$. The testing results show that J-S divergence and 128-bin histograms can improve the performance by about 2%, in contrast to the symmetric form on the basis of arithmetic geometry and harmonic means.

2.5 Multiple Information Measurement Fusion

It is difficult to acquire ideal results by using one type of IM. In this paper, we systematically introduce one local IM and two global IMs, making the obtained IQA results close to the HVS perception. The final IQA result can be obtained via a linear function:

$$\text{MMFM} = \frac{D + \beta_1 [D'_{\text{KL}}(I_R) - D'_{\text{KL}}(I_C)] + \beta_2 [D_{\text{JS}}(I_R) - D_{\text{JS}}(I_C)]}{1 + \beta_1 + \beta_2} \tag{16}$$

with

$$D'_{KL}(I_R) = \frac{D_{KL}(N_R, N_O) + D_{KL}(N_O, N_R)}{2}, \tag{17}$$

$$D'_{KL}(I_C) = \frac{D_{KL}(N_C, N_O) + D_{KL}(N_O, N_C)}{2}, \tag{18}$$

$$D_{JS}(I_R) = \frac{D_{KL}(N_R, N) + D_{KL}(N_O, N)}{2}, \tag{19}$$

$$D_{JS}(I_C) = \frac{D_{KL}(N_C, N) + D_{KL}(N_O, N)}{2}, \tag{20}$$

where N_R and N_D correspond to the histogram of the reference image I_R and the corrupted image I_C respectively. By using the symmetric variant of the K-L divergence, we can obtain: 1) the distance $D'_{KL}(I_R)$ between the referenced image and its corresponding predicted image; 2) the distance $D'_{KL}(I_C)$ between the corrupted image and its corresponding predicted image. By using the J-S divergence, we can acquire: 1) the distance $D_{JS}(I_R)$ between the referenced image and its corresponding predicted image; 2) the distance $D_{JS}(I_C)$ between the corrupted image and its corresponding predicted image. β_1 and β_2 are constants, corresponding to the weight parameters of the symmetric variant of the K-L divergence and J-S divergence, respectively.

3 Experimental Results

We selected four famous IQA models, including PSNR, SSIM, FEDM and SDM, to conduct this experiment on the commonly used LIVE database. The LIVE consists of 29 reference images and 779 corrupted images destroyed by 5 distortion types. According to the suggestion introduced by the VQEG [45], we first adopt the nonlinear regression on the basis of the five-parameter logic function to acquire the objective quality value of the 5 IQA models:

$$\text{quality}(s) = \gamma_1\left(\frac{1}{2} - \frac{1}{1 + \exp[\gamma_2(e - \gamma_3)]}\right) + \gamma_4 e + \gamma_5 \tag{21}$$

where quality(s) is the mapped value of the input value s. The e represents the value of the predicted image. The free parameters $\{\gamma_1, \gamma_2, ..., \gamma_5\}$ are ascertained in the process of curve fitting. We next exploit Pearson linear correlation coefficient (PLCC), Spearman rank-order correlation coefficient (SROCC), and root mean-squared error (RMSE) to identify the performance of these 5 IQA models on the most regularly utilized LIVE database. The experimental results are shown in Table 1, 2 and 3.

It is obvious that the proposed MMFM has obtained remarkable performance, which is superior to classical FR algorithms and RR algorithms. Beyond that, the proposed MMFM has high portability and low computational complexity, since both JPEG and JP2K compression can run fast and are widely integrated into most existing applications. First, we analyze the performance of MMFM on PLCC. Compared with FR IQA, the average performance of MMFM is only 0.8%

Table 1. PLCC values of typical models and our proposed MMFM model on 5 image subsets of distinct distortion types containing JP2K, JPEG, AGWN, Blur and Fast-fading in the database of LIVE.

Pearson linear correlation coefficient (PLCC)						
Algorithm	JP2K	JPEG	AGWN	Blur	FF	Average
PSNR	0.8896	0.8879	0.9858	0.8753	0.8895	0.8893
SSIM	0.9410	0.9504	0.9695	0.8743	0.9428	0.9356
FEDM	0.9262	0.9211	0.9256	0.7359	0.8532	0.8724
SDM	0.9447	0.9569	0.9789	0.9252	0.9316	0.9475
MMFM	0.9364	0.9353	0.9518	0.7339	0.8525	0.8820

Table 2. SROCC values of typical models and our proposed MMFM model on 5 image subsets of distinct distortion types containing JP2K, JPEG, AGWN, Blur and Fastfading in the database of LIVE.

Spearman rank-order correlation coefficient (SROCC)						
Algorithm	JP2K	JPEG	AGWN	Blur	FF	Average
PSNR	0.8954	0.8809	0.9854	0.7823	0.8907	0.8869
SSIM	0.9355	0.9449	0.9629	0.8944	0.9413	0.9358
FEDM	0.9200	0.9226	0.9152	0.7594	0.8229	0.8681
SDM	0.9439	0.9227	0.9729	0.9342	0.9384	0.9468
MMFM	0.9303	0.9323	0.9243	0.7627	0.8261	0.8751

Table 3. RMSE values of typical models and our proposed MMFM model on 5 image subsets of distinct distortion types containing JP2K, JPEG, AGWN, Blur and Fast-fading in the database of LIVE.

Root mean-squared error (RMSE)						
Algorithm	JP2K	JPEG	AGWN	Blur	FF	Average
PSNR	11.017	14.653	4.7027	11.478	13.015	10.973
SSIM	8.5349	9.9070	6.8533	8.9643	9.4963	8.7512
FEDM	9.5226	12.409	10.613	12.516	15.410	12.094
SDM	8.2737	9.2445	5.7166	7.0095	10.357	8.1202
MMFM	8.8515	11.274	8.5827	12.546	14.890	11.229

behind that of the full reference algorithm PSNR. Compared with RR IQA, the proposed MMFM achieves an average performance gain of 0.9% over FEDM. Then, the performance of MMFM on SROCC is analyzed. Compared to the FR IQA, MMFM is particularly close to the results of PSNR with an average performance, lagging only 1.3% in average performance. With respect to the RR IQA algorithm, the proposed MMFM achieves a maximum of 0.8% average performance gain over FEDM. Finally, we analyze the results obtained on RMSE. Compared with FR IQA, the average performance of MMFM algorithm is 2.3% lower than the PSNR. Compared with RR IQA, the proposed MMFM has a maximum average performance gain of 7.1% over FEDM.

Thus we would like to emphasize that: 1) MMFM obtains desirable results without increasing the computational complexity, 2) MMFM adaptively selects JPEG or JPEG2000 compression depending on the conditions of application, and 3) MMFM requires only one number and encodes that number precisely in the header file, allowing MMFM to be considered as a blind IQA model.

4 Application

Along with the speedy advancement of image processing technology, IQA models using a modest number of parameters can be expanded to various practical application scenarios. These include: 1) The monitoring methods of abnormal conditions, especially smoke monitoring in industrial scenarios, has emerged a lot of research achievements [46–48]. The detection of anomalies is extremely image dependent. The information provided by the images enables the staff to detect the target in time to avoid environmental pollution, safety accidents and a host of other problems. 2) The monitoring and early warning methods of air pollution [49,50] rely on the numerous visual features about the target provided by the images to facilitate real-time pollution monitoring. 3) 3-dimensional vision and display technologies [51] expand the image from a 2D plane to a 3D space, which can give the viewer a sense of immersion. As shown above, IQA has a wide range of applications, and in the future we will consider enhancing our algorithm to expand its applications and reap certain social and economic benefits.

5 Conclusion

In this paper, we have presented a novel IQA algorithm based on the fusion of multiple IMs from the local and global perspective. First, we have combined the AR model with sparse random sampling method to generate the predicted image corresponding to the input image. Second, we have obtained the local IM and two global IMs to measure the difference between the input image and the predicted image. Third, we have utilized the local IM and two global IMs to calculate the difference between the reference and corrupted image, and fuse the three components by a linear function. The final experimental results on the typically utilized LIVE database indicate that the MMFM has obtained competitive performance with the commonly used FR and RR IQA models.

References

1. Bovik, A.C.: Automatic prediction of perceptual image and video quality. Proc. IEEE **101**(9), 2008–2024 (2013)
2. Gu, K., et al.: Saliency-guided quality assessment of screen content images. IEEE Trans. Multimedia **18**(6), 1098–1110 (2016)
3. Gu, K., Wang, S., Zhai, G., Ma, S., Lin, W.: Screen image quality assessment incorporating structural degradation measurement. In: IEEE International Symposium on Circuits and Systems, pp. 125–128 (2015)
4. Sun, W., Gu, K., Ma, S., Zhu, W., Liu, N., Zhai, G.: A large-scale compressed 360-degree spherical image database: from subjective quality evaluation to objective model comparison. In: IEEE International Workshop on Multimedia Signal Processing, pp. 1–6 (2018)
5. Gu, K., Zhai, G., Lin, W., Liu, M.: The analysis of image contrast: from quality assessment to automatic enhancement. IEEE Trans. Cybern. **46**(1), 284–297 (2016)
6. Sheikh, H.R., Wang, Z., Cormack, L., Bovik, A.C.: LIVE image quality assessment database release 2. http://live.ece.utexas.edu/research/quality
7. Wang, Z., Bovik, A.C., Sheikh, H.R., Simoncelli, E.P.: Image quality assessment: from error visibility to structural similarity. IEEE Trans. Image Process. **13**(4), 600–612 (2004)
8. Zhang, L., Zhang, L., Mou, X., Zhang, D.: FSIM: a feature similarity index for image quality assessment. IEEE Trans. Image Process. **20**(8), 2378–2386 (2011)
9. Sheikh, H.R., Bovik, A.C.: Image information and visual quality. IEEE Trans. Image Process. **15**(2), 430–444 (2006)
10. Larson, E.C., Chandler, D.M.: Most apparent distortion: full reference image quality assessment and the role of strategy. J. Electron. Imaging **19**(1), 011006 (2010)
11. Wang, Z., Li, Q.: Information content weighting for perceptual image quality assessment. IEEE Trans. Image Process. **20**(5), 1185–1198 (2011)
12. Wang, Z., Simoncelli, E.P., Bovik, A.C.: Multi-scale structural similarity for image quality assessment. In: IEEE Asilomar Conference on Signals, Systems and Computers, pp. 1398–1402 (2003)
13. Liu, A., Lin, W., Narwaria, M.: Image quality assessment based on gradient similarity. IEEE Trans. Image Process. **21**(4), 1500–1512 (2012)
14. Gu, K., Zhai, G., Yang, X., Chen, L., Zhang, W.: Nonlinear additive model based saliency map weighting strategy for image quality assessment. In: IEEE International Workshop on Multimedia Signal Processing, pp. 313–318 (2012)
15. Xia, Z., Gu, K., Wang, S., Liu, H., Kwong, S.: Toward accurate quality estimation of screen content pictures with very sparse reference information. IEEE Trans. Ind. Electron. **67**(3), 2251–2261 (2020)
16. Wu, J., Lin, W., Shi, G., Liu, A.: Perceptual quality metric with internal generative mechanism. IEEE Trans. Image Process. **22**(1), 43–54 (2013)
17. Gu, K., Zhai, G., Yang, X., Zhang, W.: Self-adaptive scale transform for IQA metric. In: Proceedings of the IEEE International Symposium on Circuits and Systems, pp. 2365–2368 (2013)
18. Wang, S., Gu, K., Zhang, X., Lin, W., Ma, S., Gao, W.: Reduced reference quality assessment of screen content images. IEEE Trans. Circuits Syst. Video Technol. **28**(1), 1–14 (2018)
19. Gu, K., Zhai, G., Yang, X., Zhang, W., Liu, M.: Structural similarity weighting for image quality assessment. In: Proceedings of the IEEE International Conference on Multimedia and Expo Workshops, pp. 1–6 (2013)

20. Chen, W., Gu, K., Min, X., Yuan, F., Cheng, E., Zhang, W.: Partial-reference sonar image quality assessment for underwater transmission. IEEE Trans. Aerosp. and Electron. Syst. **54**(6), 2776–2787 (2018)
21. Zhai, G., Wu, X., Yang, X., Lin, W., Zhang, W.: A psychovisual quality metric in free-energy principle. IEEE Trans. Image Process. **21**(1), 41–52 (2012)
22. Gu, K., Zhai, G., Yang, X., Zhang, W., Liu, M.: Subjective and objective quality assessment for images with contrast change. In: Proceedings of the IEEE International Conference on Image Processing, pp. 383–387 (2013)
23. Narwaria, M., Lin, W., McLoughlin, I.V., Emmanuel, S., Chia, L.T.: Fourier transform-based scalable image quality measure. IEEE Trans. Image Process. **21**(8), 3364–3377 (2012)
24. Gu, K., Zhai, G., Yang, X., Zhang, W.: A new reduced-reference image quality assessment using structural degradation model. In: Proceedings of the IEEE International Symposium on Circuits and Systems, pp. 1095–1098 (2013)
25. Rehman, A., Wang, Z.: Reduced-reference image quality assessment by structural similarity estimation. IEEE Trans. Image Process. **21**(8), 3378–3389 (2012)
26. Soundararajan, R., Bovik, A.C.: RRED indices: reduced-reference entropic differencing for image quality assessment. IEEE Trans. Image Process. **21**(2), 517–526 (2012)
27. Gu, K., Zhai, G., Lin, W., Yang, X., Zhang, W.: No-reference image sharpness assessment in autoregressive parameter space. IEEE Trans. Image Process. **24**(10), 3218–3231 (2015)
28. Mittal, A., Moorthy, A.K., Bovik, A.C.: No-reference image quality assessment in the spatial domain. IEEE Trans. Image Process. **21**(12), 4695–4708 (2012)
29. Gu, K., Zhou, J., Qiao, J., Zhai, G., Lin, W., Bovik, A.C.: No-reference quality assessment of screen content pictures. IEEE Trans. Image Process. **26**(8), 4005–4018 (2017)
30. Gu, K., Lin, W., Zhai, G., Yang, X., Zhang, W., Chen, C.W.: No-reference quality metric of contrast-distorted images based on information maximization. IEEE Trans. Cybern. **47**(12), 4559–4565 (2017)
31. Min, X., Gu, K., Zhai, G., Liu, J., Yang, X., Chen, C.W.: Blind quality assessment based on pseudo-reference image. IEEE Trans. Multimedia **20**(8), 2049–2062 (2018)
32. Gu, K., Zhai, G., Yang, X., Zhang, W.: Deep learning network for blind image quality assessment. In: IEEE International Conference on Image Processing, pp. 511–515 (2014)
33. Gu, K., Tao, D., Qiao, J., Lin, W.: Learning a no-reference quality assessment model of enhanced images with big data. IEEE Trans. Neural Netw. Learn. Syst. **29**(4), 1301–1313 (2018)
34. Gu, K., Zhai, G., Yang, X., Zhang, W.: Using free energy principle for blind image quality assessment. IEEE Trans. Multimedia **17**(1), 50–63 (2015)
35. Zhang, L., Zhang, L., Bovik, A.C.: A feature-enriched completely blind image quality evaluator. IEEE Trans. Image Process. **24**(8), 2579–2591 (2015)
36. Gu, K., et al.: Blind quality assessment of tone-mapped images via analysis of information, naturalness, and structure. IEEE Trans. Multimedia **18**(3), 432–443 (2016)
37. Gu, K., Li, L., Lu, H., Min, X., Lin, W.: A fast reliable image quality predictor by fusing micro- and macro-structures. IEEE Trans. Ind. Electron. **64**(5), 3903–3912 (2017)
38. Gu, K., Zhai, G., Yang, X., Zhang, W.: Hybrid no-reference quality metric for singly and multiply distorted images. IEEE Trans. Broadcast. **60**(3), 555–567 (2014)

39. Friston, K., Kilner, J., Harrison, L.: A free energy principle for the brain. J. Physiol. Paris **100**, 70–87 (2006)
40. Friston, K.: The free-energy principle: a unified brain theory? Nat. Rev. Neurosci. **11**, 127–138 (2010)
41. Yue, G., Hou, C., Gu, K., Zhou, T., Zhai, G.: Combining local and global measures for DIBR-synthesized image quality evaluation. IEEE Trans. Image Process. **28**(4), 2075–2088 (2019)
42. Knill, D.C., Pouget, A.: The Bayesian brain: the role of uncertainty in neural coding and computation. Trends Neurosci. **27**(12), 712–719 (2004)
43. Attias, H.: A variational Bayesian framework for graphical models. Adv. Neural. Inf. Process. Syst. **12**, 209–215 (2000)
44. Johnson, D.H., Sinanovic, S.: Symmetrizing the Kullback-Leibler distance. IEEE Trans. Inf. Theory (2001)
45. VQEG: Final report from the video quality experts group on the validation of objective models of video quality assessment (2000). http://www.vqeg.org/
46. Gu, K., Zhang, Y., Qiao, J.: Ensemble meta-learning for few-shot soot density recognition. IEEE Trans. Ind. Informat. **17**(3), 2261–2270 (2021)
47. Gu, K., Xia, Z., Qiao, J., Lin, W.: Deep dual-channel neural network for image based smoke detection. IEEE Trans. Multimedia **22**(2), 311–323 (2020)
48. Liu, H., Lei, F., Tong, C., Cui, C., Wu, L.: Visual smoke detection based on ensemble deep CNNs. Displays **69**, 102020 (2021)
49. Gu, K., Liu, H., Xia, Z., Qiao, J., Lin, W., Thalmann, D.: $PM_{2.5}$ monitoring: use information abundance measurement and wide and deep learning. IEEE Trans. Neural Netw. Learn. Syst. **32**(10), 4278–4290 (2021)
50. Gu, K., Xia, Z., Qiao, J.: Stacked selective ensemble for $PM_{2.5}$ forecast. IEEE Trans. Instrum. Meas. **69**(3), 660–671 (2020)
51. Ye, P., Wu, X., Gao, D., Deng, S., Xu, N., Chen, J.: DP3 signal as a neuro indictor for attentional processing of stereoscopic contents in varied depths within the 'comfort zone'. Displays **63**, 101953 (2020)